

# Influence of Fermi surface topology on the quasiparticle spectrum in the vortex state

S. Graser, T. Dahm, and N. Schopohl  
*Institut für Theoretische Physik, Universität Tübingen,  
Auf der Morgenstelle 14, D-72076 Tübingen, Germany*  
(Dated: October 3, 2018)

We study the influence of Fermi surface topology on the quasiparticle density of states in the vortex state of type II superconductors. We observe that the field dependence and the shape of the momentum and spatially averaged density of states is affected significantly by the topology of the Fermi surface. We show that this behavior can be understood in terms of characteristic Fermi surface functions and that an important role is played by the number of points on the Fermi surface at which the Fermi velocity is directed parallel to the magnetic field. A critical comparison is made with a broadened BCS type density of states, that has been used frequently in analysis of tunneling data. We suggest a new formula as a replacement for the broadened BCS model for the special case of a cylindrical Fermi surface. We apply our results to the two gap superconductor  $\text{MgB}_2$  and show that in this particular case the field dependence of the partial densities of states of the two gaps behaves very differently due to the different topologies of the corresponding Fermi surfaces, in qualitative agreement with recent tunneling experiments.

PACS numbers: 74.25.Op, 71.18.+y, 74.50.+r, 74.70.Ad

## I. INTRODUCTION

The quasiparticle density of states is one of the characteristic properties of a superconductor. It contains information about the gap function and can be probed by various experimental techniques such as tunneling spectroscopy, photoemission, specific heat, nuclear magnetic resonance (NMR) etc. These techniques are often used to extract information about the superconducting gap in a given system. Recently, there is growing interest to study the quasiparticle excitations in the vortex state of type II superconductors, particularly in unconventional superconductors.<sup>1,2,3,4,5,6,7</sup> For example, the zero energy density of states in a  $d$ -wave superconductor is expected to vary as the square-root of the magnetic field  $B$  instead of the linear  $B$ -field variation expected in a dirty  $s$ -wave superconductor.<sup>8,9,10</sup> However, the relation between the gap function and the quasiparticle density of states is less direct in the vortex state than in the Meissner state. The reason is that there are important modifications of the density of states due to bound states in the vortex cores and the supercurrents running around the vortices, particularly at higher magnetic fields. In this case quasiparticles are excited with respect to the local supercurrent flow and their energy appears 'Doppler-shifted'.<sup>11</sup> In analysis of tunneling spectra these effects are often modeled as a 'smearing effect' of the zero field density of states.<sup>4,5,7</sup> However, as we will show below, the quasiparticle excitations above the moving supercurrent contain information about the momentum dependent Fermi velocity, especially its direction relative to the applied magnetic field. For this reason the particular shape of the Fermi surface has an important influence on the momentum averaged quasiparticle density of states in the vortex state.

Here, we want to present a detailed study of this in-

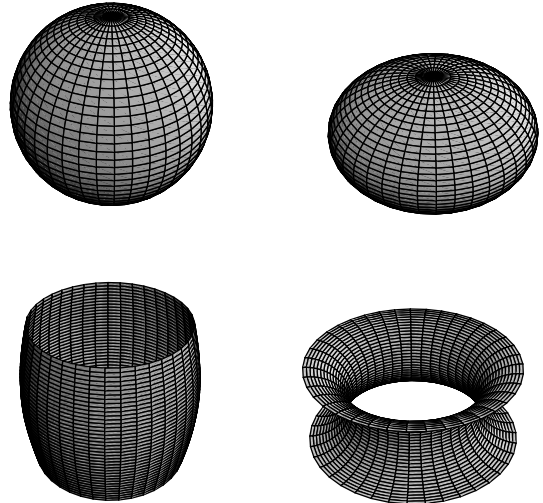


FIG. 1: Different shapes of the Fermi surface that are investigated within this work. In the upper row we have on the left hand side a spherical Fermi surface and on the right hand side an elliptical Fermi surface. In the lower row we show on the left hand side a distorted cylinder with a distortion parameter  $\epsilon_c = 0.163$  and on the right hand side a half-torus.

fluence of the Fermi surface structure on the quasiparticle density of states in the vortex state. We are going to compare the different Fermi surface types shown in Fig. 1: spherical and elliptical Fermi surfaces as they are used commonly in isotropic and anisotropic effective mass models, a cylindrical Fermi surface with a small  $c$ -axis dispersion as appropriate for layered systems, and a Fermi surface of half-torus shape which is relevant for the

$\pi$ -band in the recently discussed superconductor  $\text{MgB}_2$ , for example.<sup>12</sup> Our calculations are based on quasiclassical Eilenberger theory using a method that was originally introduced by Pesch<sup>13</sup> to describe type II superconductors at high magnetic fields and that we have generalized to unconventional pairing symmetry recently.<sup>14</sup> In that work we have shown that this method leads to much more accurate results than the frequently used 'Doppler-shift method', particularly at higher magnetic fields, mainly because it takes into account the contributions from vortex core states properly. Our results presented below show that the structure of the Fermi surface affects the density of states in the presence of a magnetic field quite dramatically. We are going to describe our calculational procedure in section II. In section III we introduce the different Fermi surface types used in the present study. Section IV contains our results and interpretation in terms of characteristic Fermi surface functions. In section V we compare our results with the model of a broadened BCS type density of states that has been used frequently for analysis of experimental data. In section VI we study the particularly interesting case of the two gap superconductor  $\text{MgB}_2$ , which possesses four Fermi surfaces of two different types: two cylindrical  $\sigma$ -bands and two  $\pi$ -bands, which can be modeled by the half-torus in Fig. 1.<sup>12</sup> These different Fermi surface types lead to very different field dependencies of the partial densities of states for the two gaps.

## II. QUASIPARTICLE SPECTRUM IN THE VORTEX STATE

Our calculation of the quasiparticle spectrum in the vortex state is based on quasiclassical Eilenberger theory.<sup>15,16</sup> As we have shown in Ref. 14 there exists an accurate approximate method for the calculation of the density of states averaged over a unit cell of the vortex lattice (see section IV.A in Ref. 14) and we briefly repeat the essential equations here. We start from the Eilenberger equation for the normal and anomalous component  $g$  and  $f$  of the quasiparticle propagator of a spin-singlet superconductor<sup>15,16</sup>

$$\left[ 2 \left( i\epsilon_n + \frac{e}{c} \vec{v}_F \cdot \vec{A} \right) + i\hbar \vec{v}_F \cdot \vec{\nabla} \right] f(\vec{r}, \vec{k}_F, i\epsilon_n) = 2ig(\vec{r}, \vec{k}_F, i\epsilon_n) \Delta(\vec{r}, \vec{k}_F) \quad (1)$$

Here,  $\vec{A}$  is the vector potential and is chosen to be  $\vec{A} = -\frac{1}{2} \vec{r} \times \vec{B}$ , the vector  $\vec{v}_F = \vec{v}_F(\vec{k}_F)$  denotes the Fermi velocity at the momentum point  $\vec{k}_F$  at the Fermi surface and  $\epsilon_n$  are the fermionic Matsubara frequencies. Eq. (1) has to be supplemented by a normalization condition<sup>15</sup>

$$\left[ g(\vec{r}, \vec{k}_F, i\epsilon_n) \right]^2 + f(\vec{r}, \vec{k}_F, i\epsilon_n) f^*(\vec{r}, -\vec{k}_F, i\epsilon_n) = 1 \quad (2)$$

For the spatial variation of the gap function  $\Delta(\vec{r}, \vec{k}_F) = \Delta(\vec{k}_F) \cdot \psi_\Lambda(x, y)$  we take the Abrikosov vortex lattice in

the following form<sup>14</sup>

$$\psi_\Lambda(x, y) = \frac{1}{\mathcal{N}} \sum_{n=-\infty}^{\infty} \exp \left[ \frac{\pi (ixy - y^2)}{\omega_1 \text{Im} \omega_2} + i\pi n + \frac{i\pi(2n+1)}{\omega_1} (x + iy) + i\pi \frac{\omega_2}{\omega_1} n(n+1) \right] \quad (3)$$

where  $x$  and  $y$  are the coordinates in the plane perpendicular to the magnetic field  $\vec{B}$  and the complex quantities  $\omega_1$  and  $\omega_2$  span the vortex lattice  $\Lambda$ .  $\mathcal{N}$  is a normalization factor that has to be chosen in such a way that  $|\psi_\Lambda|^2$  averaged over a unit cell of  $\Lambda$  equals unity. The normalized local density of states can be obtained from the real part of the analytical continuation of  $g$ , averaged over the Fermi surface

$$N(\vec{r}, E) = \left\langle \text{Re} \left\{ g(\vec{r}, \vec{k}_F, E + i0^+) \right\} \right\rangle_{FS} \quad (4)$$

where

$$\left\langle \dots \right\rangle_{FS} = \frac{1}{N(0)} \int_{FS} \frac{d^2 k_F}{(2\pi)^3} \frac{1}{|\hbar \vec{v}_F(\vec{k}_F)|} \dots \quad (5)$$

denotes an average over the Fermi surface.

Proceeding along the lines in Ref. 14 we can now find the following approximate analytical solution for the density of states spatially averaged over a unit cell  $C_\Lambda$  of the vortex lattice for arbitrary field directions:

$$g(\vec{k}_F, i\epsilon_n) = \frac{1}{|C_\Lambda|} \int_{C_\Lambda} d^2 r g(\vec{r}, \vec{k}_F, i\epsilon_n) = \frac{1}{\sqrt{1 + P_\Lambda(\vec{k}_F, i\epsilon_n)}} \quad (6)$$

where the momentum and frequency dependent function  $P_\Lambda$  takes the form

$$P_\Lambda(\vec{k}_F, i\epsilon_n) = \frac{4|\Delta(\vec{k}_F)|^2}{|\eta_{k_F}|^2} (1 - \sqrt{\pi} z w(iz)) \quad (7)$$

The  $w$ -function, also known as Dawson's integral, is related to the complement of the Error function by

$$w(iz) = \frac{1}{i\pi} \int_{-\infty}^{\infty} \frac{e^{-t^2}}{t - iz} dt = e^{z^2} \text{erfc}(z) \quad (8)$$

Furthermore  $z$  are normalized Matsubara frequencies of the following form

$$z = \frac{\sqrt{2}\epsilon_n}{|\eta_{k_F}|} \quad (9)$$

where  $\eta_{k_F}$  is proportional to the projection of the Fermi velocity into the complex plane perpendicular to the magnetic field direction and given by

$$\eta_{k_F} = \hbar(v_{F,1} + iv_{F,2}) \sqrt{\frac{eB}{\hbar c}} \quad (10)$$

Here,  $v_{F,1}$  and  $v_{F,2}$  are the components of the Fermi velocity in the plane perpendicular to the average magnetic field  $\vec{B}$ . Using the flux quantization condition

$$\frac{\pi}{\omega_1 \text{Im } \omega_2} = \frac{eB}{\hbar c} \quad (11)$$

where  $\omega_1 \text{Im } \omega_2 = |C_\Lambda|$  is the size of a unit cell of the vortex lattice (if we assume  $\omega_1$  to be real) we can bring  $\eta_{k_F}$  into the form

$$\eta_{k_F} = \hbar(v_{F,1} + iv_{F,2}) \sqrt{\frac{\pi}{\omega_1 \text{Im } \omega_2}} \quad (12)$$

If the magnetic field is not directed parallel to the  $c$ -axis of the uniaxial systems considered here, then the rotational symmetry around the magnetic field direction is broken and we have to take into account, that the isotropic vortex lattice no longer has to be the appropriate ground state. If we use a variational ansatz for a distorted Abrikosov vortex lattice with

$$\psi_\Lambda^\tau(x, y) = \psi_\Lambda(e^{-\tau}x, e^\tau y) \quad (13)$$

we find that the Fermi velocity components in Eq. (10) have to be replaced by the scaled Fermi velocities<sup>12</sup>

$$\tilde{v}_{F,1} = e^\tau v_{F,1}, \quad \text{and} \quad \tilde{v}_{F,2} = e^{-\tau} v_{F,2} \quad (14)$$

The distortion parameter  $\tau$  has to be found by a minimization of the free energy at a given field strength and temperature.

Within our approximation the free energy difference between superconducting and normal state is given by the expression

$$\Omega_S - \Omega_N = - \left\langle \pi T \sum_{|\epsilon_n| < \omega_c} \frac{|\Delta(\vec{k}_F)|^2}{\epsilon_n} \sqrt{\pi} z w(iz) \right. \quad (15)$$

$$\left. \text{Re} \left[ \frac{P_\Lambda(\vec{k}_F, i\epsilon_n)}{\sqrt{1 + P_\Lambda(\vec{k}_F, i\epsilon_n)} \left(1 + \sqrt{1 + P_\Lambda(\vec{k}_F, i\epsilon_n)}\right)^2} \right] \right\rangle_{FS}$$

A derivation of this expression can be found in Appendix A. For each value of  $\tau$  the gap function in Eq. (15) has to be calculated from the gap equation

$$\left\langle \pi T \sum_{|\epsilon_n| < \omega_c} \frac{|\Delta(\vec{k}_F)|^2}{\epsilon_n} \left[ g(\vec{k}_F, i\epsilon_n) \sqrt{\pi} z w(iz) - 1 \right] \right. \\ \left. - |\Delta(\vec{k}_F)|^2 \ln \frac{T}{T_c} \right\rangle_{FS} = 0 \quad (16)$$

self-consistently. We note that the variational parameter  $\tau$  enters Eqs. (15) and (16) only via the quantity  $|\eta_{k_F}(\tau)|$ . A determination of  $\tau$  requires to minimize Eq. (15), where for each trial value of  $\tau$  Eq. (16) has to be solved self-consistently. Fortunately, we were able

to find analytical results for  $\tau$  in some of the cases studied below, such that this minimization procedure could be avoided in these cases.

The field dependent total density of states averaged over the Fermi surface and a unit cell of the vortex lattice is found from Eq. (6)

$$N(B, E) = \left\langle \text{Re} \left\{ \frac{1}{\sqrt{1 + P_\Lambda(\vec{k}_F, E + i0^+)}} \right\} \right\rangle_{FS} \quad (17)$$

We note that the direction of the Fermi velocity enters this equation only via the quantity  $|\eta_{k_F}|$  and that only the components perpendicular to the magnetic field play a role. This is where the Fermi surface structure comes into play.

### III. PARAMETRIZATION OF THE FERMI SURFACE

In order to parametrize the different Fermi surfaces we have to find an appropriate parametrization of the Fermi wave vector  $\vec{k}_F$ :

$$\vec{k}_F(\vartheta, \varphi) = k_x(\vartheta, \varphi) \vec{e}_x + k_y(\vartheta, \varphi) \vec{e}_y + k_z(\vartheta, \varphi) \vec{e}_z \quad (18)$$

Using this parametrization we can calculate the outward oriented normal unit vector  $\vec{n}_F$

$$\vec{n}_F = \frac{\vec{t}_\varphi \times \vec{t}_\vartheta}{|\vec{t}_\varphi \times \vec{t}_\vartheta|} \quad (19)$$

where  $\vec{t}_\varphi$  and  $\vec{t}_\vartheta$  are two orthogonal tangential vectors that are parallel to the coordinate lines of  $\varphi$  and  $\vartheta$

$$\vec{t}_\varphi = \partial_\varphi \vec{k}_F(\vartheta, \varphi), \quad \vec{t}_\vartheta = \partial_\vartheta \vec{k}_F(\vartheta, \varphi) \quad (20)$$

The Fermi velocity vector is always directed perpendicular to the Fermi surface and thus can be written in general as

$$\vec{v}_F = v_F \cdot \vec{n}_F \quad (21)$$

The Fermi surface of layered systems as for example the high  $T_c$ -cuprates can be described as a distorted cylinder. The distortion is due to a small  $c$ -axis dispersion. In this case we can parametrize the distorted cylindrical Fermi surface as

$$k_x(k_c, \varphi) = \left( k_{ab} + \frac{\epsilon_c}{c} \cos(ck_c) \right) \cos \varphi, \\ k_y(k_c, \varphi) = \left( k_{ab} + \frac{\epsilon_c}{c} \cos(ck_c) \right) \sin \varphi, \\ k_z(k_c, \varphi) = k_c \quad (22)$$

with a dimensionless  $c$ -axis dispersion parameter  $\epsilon_c$ . The parameter  $k_c$  is running from  $-\pi/c$  to  $\pi/c$  where  $c$  is the lattice constant in  $c$ -axis direction. The polar angle  $\varphi$  varies in the interval  $[0, 2\pi]$ .

Another Fermi surface that we will discuss is a half-torus. In magnesium diboride with its hexagonal crystal structure the  $\pi$ -band possesses a tubular Fermi surface structure that can be approximated by a half-torus living at the border of the hexagonal unit cell of the reciprocal lattice.<sup>12</sup> In this case we have the following parametrization

$$\begin{aligned} k_x(\vartheta, \varphi) &= k_F \cdot (\nu + \cos \vartheta) \cos \varphi, \\ k_y(\vartheta, \varphi) &= k_F \cdot (\nu + \cos \vartheta) \sin \varphi, \\ k_z(\vartheta, \varphi) &= k_F \cdot \sin \vartheta \end{aligned} \quad (23)$$

where the parameter  $\nu$  denotes the ratio between the radius of the meridian and the radius of the longitudinal curve of the torus. Again  $\varphi$  can take values between 0 and  $2\pi$  while  $\vartheta$  varies between  $\pi/2$  and  $3\pi/2$  to parametrize the concave half-torus. The spherical Fermi surface can be viewed as a special case of the toroidal Fermi surface with parameter  $\nu = 0$ .

If we assume a crystal with different effective masses in the  $c$ -axis direction and within the  $ab$ -plane

$$\epsilon_k = \frac{1}{2m_{ab}}(k_a^2 + k_b^2) + \frac{1}{2m_c}k_c^2 - \epsilon_F \quad (24)$$

we find an elliptic Fermi surface with the following parametrization

$$\begin{aligned} k_x(\vartheta, \varphi) &= k_F \cdot \cos \vartheta \cos \varphi, \\ k_y(\vartheta, \varphi) &= k_F \cdot \cos \vartheta \sin \varphi, \\ k_z(\vartheta, \varphi) &= k_F \cdot \sqrt{m_c/m_{ab}} \sin \vartheta \end{aligned} \quad (25)$$

Here,  $\vartheta$  takes values between  $-\pi/2$  and  $\pi/2$ . In Fig. 1 we show the four different Fermi surfaces discussed above. From these parametrizations we can now calculate the Fermi velocity and its projection into the plane perpendicular to the magnetic field. We will consider the two cases of a magnetic field applied parallel to the  $c$ -axis direction of the crystal and the case of an in plane magnetic field.

For the cylinder with  $c$ -axis dispersion  $\epsilon_c$  we assume that  $\epsilon_c^2 \ll 1$ . In this case the variation of the in-plane components of the Fermi velocity due to the  $c$ -axis dispersion can be neglected. Then we can write

$$\vec{v}_F = v_F(\cos \varphi \vec{e}_x + \sin \varphi \vec{e}_y + \epsilon_c \sin \varphi k_c \vec{e}_z) \quad (26)$$

For the half-torus and the sphere the Fermi velocity is found to be:

$$\vec{v}_F = v_F(\cos \varphi \cos \vartheta \vec{e}_x + \sin \varphi \cos \vartheta \vec{e}_y + \sin \vartheta \vec{e}_z) \quad (27)$$

Writing  $v_{F,ab} = k_F/m_{ab}$  and  $v_{F,c} = k_F/\sqrt{m_c m_{ab}}$  we find for the elliptical Fermi surface:

$$\begin{aligned} \vec{v}_F &= \vec{\nabla}_k \epsilon_k = \\ &v_{F,ab}(\cos \varphi \cos \vartheta \vec{e}_x + \sin \varphi \cos \vartheta \vec{e}_y) + v_{F,c} \sin \vartheta \vec{e}_z \end{aligned} \quad (28)$$

The Fermi surface average Eq. (5) reads in these coordinates

$$\langle \dots \rangle_{FS} = \frac{c}{4\pi^2} \int_0^{2\pi} d\phi \int_{-\pi/c}^{\pi/c} dk_c \dots \quad (29)$$

for the cylindrical Fermi surface with  $\epsilon_c^2 \ll 1$  and

$$\langle \dots \rangle_{FS} = \frac{1}{2\pi} \int_0^{2\pi} d\phi \int_{\pi/2}^{3\pi/2} d\vartheta \frac{\nu + \cos \vartheta}{\pi\nu - 2} \dots \quad (30)$$

for the half-torus. The integrations for spherical and elliptical Fermi surface are obtained from Eq. (30) for  $\nu = 0$ .

### A. Field in $c$ -axis direction

As pointed out above, for the calculation of the density of states in the vortex state using Eq. (17) we only need to know the modulus of the quantity  $\eta_{k_F}$  introduced in section II. This quantity only contains the components of the Fermi velocity perpendicular to the external magnetic field. For field directed in  $c$ -axis direction we therefore only need the  $ab$ -plane components. As a result of the rotational symmetry of all the Fermi surfaces considered we expect no angular dependence on the polar angle  $\varphi$ . For the cylindrical Fermi surface we find no angular dependence at all

$$|\eta_{k_F}| = \hbar v_F \sqrt{\frac{eB}{\hbar c}} \quad (31)$$

For the toroidal or the spherical Fermi surface a dependence on the azimuthal angle  $\vartheta$  is found:

$$|\eta_{k_F}| = \hbar v_F |\cos \vartheta| \sqrt{\frac{eB}{\hbar c}} \quad (32)$$

For the elliptic Fermi surface we have

$$|\eta_{k_F}| = \hbar v_{F,ab} |\cos \vartheta| \sqrt{\frac{eB}{\hbar c}} \quad (33)$$

### B. Field in $ab$ -plane direction

If we consider a magnetic field that is not parallel to the  $c$ -axis direction, the rotational symmetry around the  $c$ -axis is broken and we find more complicated expressions for the Fermi velocity projection  $\eta_{k_F}$ . In this case we can find the projection by a simple rotation, for example around the  $a$ -axis. If we carry out a rotation with angle  $\gamma$  we obtain a modified expression for the Fermi velocity in the rotated coordinate frame

$$\begin{aligned} \vec{v}'_F &= v_{F,a} \vec{e}_1 + (\cos \gamma v_{F,b} - \sin \gamma v_{F,c}) \vec{e}_2 \\ &+ (\sin \gamma v_{F,b} + \cos \gamma v_{F,c}) \vec{e}_3 \end{aligned} \quad (34)$$

Here the unit vector  $\vec{e}_3$  is chosen to point into the direction of the magnetic field and  $\vec{e}_1, \vec{e}_2$  span the plane perpendicular to the magnetic field.  $v_{F,a}, v_{F,b}$  and  $v_{F,c}$  are the components of the Fermi velocity along the  $a$ -,  $b$ - and  $c$ -axis of the crystal, respectively. If the magnetic field is applied along the  $ab$ -plane direction of the crystal,

the angle  $\gamma$  equals  $\pi/2$  and the Fermi velocity  $\vec{v}'_F$  in the rotated coordinate frame can be written as

$$\vec{v}'_F = v_{F,a}\vec{e}_1 + (-v_{F,c})\vec{e}_2 + v_{F,b}\vec{e}_3 \quad (35)$$

As we have pointed out above, in this field direction the distortion of the vortex lattice has to be taken into account which leads to a scaling of the components of the Fermi velocity (see Eq. (14)). In this way we find for the cylindrical Fermi surface

$$|\eta_{k_F}| = \hbar v_F \sqrt{\frac{eB}{\hbar c}} \sqrt{e^{2\tau} \cos^2 \varphi + e^{-2\tau} \epsilon_c^2 \sin^2 \varphi}, \quad (36)$$

for half-torus and sphere we have

$$|\eta_{k_F}| = \hbar v_F \sqrt{\frac{eB}{\hbar c}} \sqrt{e^{2\tau} \cos^2 \varphi \cos^2 \vartheta + e^{-2\tau} \sin^2 \vartheta}, \quad (37)$$

and for the elliptical Fermi surface we find

$$|\eta_{k_F}| = \hbar \sqrt{\frac{eB}{\hbar c}} \sqrt{e^{2\tau} v_{F,ab}^2 \cos^2 \varphi \cos^2 \vartheta + e^{-2\tau} v_{F,c}^2 \sin^2 \vartheta} \quad (38)$$

In this case it is useful to introduce a rescaling of the distortion parameter  $\tau$  via

$$e^{\bar{\tau}} = e^{\tau} \sqrt{\frac{v_{F,ab}}{v_{F,c}}} \quad (39)$$

Then we can write

$$|\eta_{k_F}| = \hbar \sqrt{v_{F,ab} v_{F,c}} \sqrt{\frac{eB}{\hbar c}} \sqrt{e^{2\bar{\tau}} \cos^2 \varphi \cos^2 \vartheta + e^{-2\bar{\tau}} \sin^2 \vartheta} \quad (40)$$

This equation has the same form as Eq. (37) with  $\tau$  being replaced by  $\bar{\tau}$  and  $v_F$  by  $\sqrt{v_{F,ab} v_{F,c}}$ . In the next section these expressions are used for evaluation of the Fermi surface integration and calculation of the spatially and momentum averaged density of states.

#### IV. FERMION SURFACE INTEGRATION

In order to calculate the quasiparticle spectrum, we have to integrate the spatially averaged density of states over the Fermi surface using Eq. (17). In the following we are going to discuss the case of an isotropic  $s$ -wave gap and the two gap superconductor MgB<sub>2</sub>. Some results for a  $d$ -wave gap and a cylindrical Fermi surface can be found in our previous work.<sup>14</sup> We note that for an isotropic  $s$ -wave gap the function  $P_\Lambda$  depends on momentum  $\vec{k}_F$  only via the quantity  $|\eta_{k_F}|$ . In this case it is useful to introduce a characteristic Fermi surface function  $g_F(s)$  of the following form

$$g_F(s) = \frac{1}{N(0)} \int_{FS} \frac{d^2 k_F}{(2\pi)^3} \frac{1}{|\hbar \vec{v}'_F(\vec{k}_F)|} \delta\left(s - \frac{|\eta_{k_F}|}{\alpha}\right) \quad (41)$$

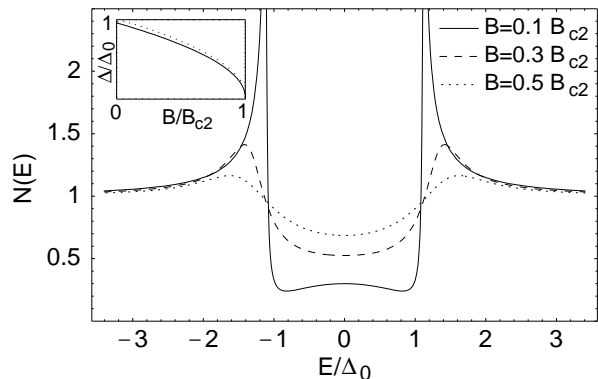


FIG. 2: Averaged density of states in the vortex state for the cylindrical Fermi surface with magnetic field in  $c$ -axis direction for three different magnetic fields  $B/B_{c2} = 0.1, 0.3,$  and  $0.5$ . The inset shows the field dependence of the gap amplitude in units of  $\Delta_0$  obtained numerically from Eq. (16) (dots) and the approximation Eq. (48) (solid line).

For convenience, we have introduced a parameter  $\alpha$  containing the field dependence

$$\alpha = \hbar v_F \sqrt{\frac{eB}{\hbar c}} \quad (42)$$

For a given value of  $s$ ,  $g_F(s)$  counts the number of states at the Fermi surface with a certain projection of the Fermi velocity into the plane perpendicular to the magnetic field. Using the function  $g_F(s)$  the density of states for a given value of  $\alpha$  can be written as a single integration over the variable  $s$ :

$$N(B, E) = \int_0^\infty ds g_F(s) \operatorname{Re} \left[ \frac{1}{\sqrt{1 + P_\Lambda(\alpha s, E)}} \right] \quad (43)$$

with

$$P_\Lambda(\alpha s, E) = \frac{4|\Delta|^2}{(\alpha s)^2} (1 - \sqrt{\pi} z(\alpha s) w(iz(\alpha s))) \quad (44)$$

Here,  $z(\alpha s)$  is the normalized real axis frequency

$$z(\alpha s) = \frac{-i\sqrt{2}}{\alpha s} (E + i0^+) \quad (45)$$

All information about the Fermi surface structure is contained in the function  $g_F(s)$ , which still depends on the direction of the magnetic field, but not on the magnitude. Looking at Eq. (43)  $g_F(s)$  can be interpreted as a weighting function.

##### A. Field in $c$ -axis direction

The characteristic function  $g_F(s)$  assumes a particularly simple form when the magnetic field is directed

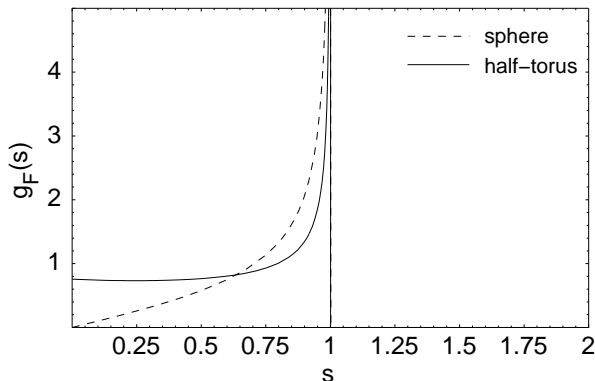


FIG. 3: The characteristic functions  $g_F(s)$  for the spherical and half-toroidal Fermi surface. The magnetic field is applied along the  $c$ -axis direction and we have chosen the ratio of the toroidal radii to be  $\nu = 4$ .

along the crystal  $c$ -axis. For the cylindrical Fermi surface  $|\eta_{k_F}|$  becomes angular independent and the characteristic function reduces to a  $\delta$ -function:

$$g_F(s) = \delta(s - 1) \quad (46)$$

In this case the density of states is just given by

$$N_{\text{cyl}}(B, E) = \text{Re} \left[ \frac{1}{\sqrt{1 + P_\Lambda(\alpha, E)}} \right] \quad (47)$$

in agreement with Eq. (36) in Ref. 14. This result is shown in Fig. 2 as a function of the quasiparticle energy  $E$  in units of the zero field gap value  $\Delta_0 = \Delta(B = 0)$  for three different field strengths. For simplicity we have used a field dependence of the gap function<sup>11</sup>

$$\Delta(B) = \Delta_0 \sqrt{1 - \frac{B}{B_{c2}}} \quad (48)$$

shown as the solid line in the inset of Fig. 2. This field dependence is a very good approximation to the field dependence obtained from the gap equation Eq. (16) numerically (solid squares in the inset).<sup>24</sup> The value of  $|\eta_{k_F}|$  at the upper critical field is found from the linearized gap equation Eq. (16) to be

$$|\eta_{k_F}|(B_{c2}) = \sqrt{2\gamma} \Delta_0 \simeq 1.887 \Delta_0 \quad (49)$$

with  $\ln \gamma = 0.577215$  being Euler's constant.

As becomes apparent from Fig. 2, the peak-to-peak distance of the gap structure in the density of states *increases* with increasing field, while the gap itself *decreases*. For this reason the gap structure seen in the density of states is not a good quantitative measure of the gap in the vortex state anymore.

Apparently, the density of states in the general case Eq. (43) can be reduced to an integral over the density

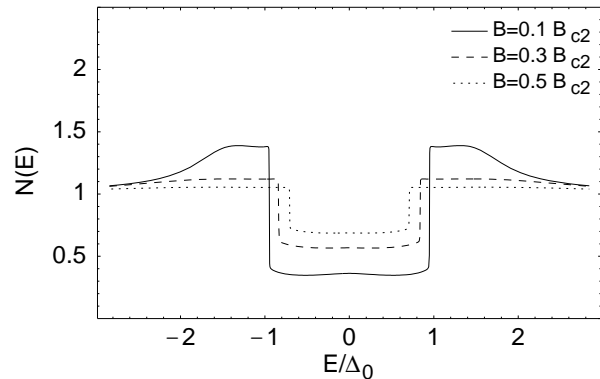


FIG. 4: Averaged density of states for the toroidal Fermi surface with magnetic field parallel to the  $c$ -axis direction

of states for the cylindrical Fermi surface Eq. (47):

$$N(B, E) = \int_0^\infty ds g_F(s) N_{\text{cyl}}(\alpha s, E) \quad (50)$$

This means that  $N(B, E)$  consists of a weighted average of the density of states for the cylindrical Fermi surface in Fig. 2 for different magnetic field strengths ranging from  $B = 0$  (corresponding to  $s = 0$ ) up to a certain upper limit given by the maximum of  $|\eta_{k_F}|$  on the Fermi surface.

For the toroidal Fermi surface the integral over the Fermi surface in Eq. (41) can be done analytically and for the characteristic function we find

$$g_F(s) = \begin{cases} \frac{\nu - s}{\pi\nu - 2} \frac{2}{\sqrt{1 - s^2}} & \text{for } 0 \leq s < 1 \\ 0 & \text{else} \end{cases} \quad (51)$$

The result for the spherical Fermi surface is obtained for  $\nu = 0$ . The same result is also found for the elliptical Fermi surface, if  $v_F$  in Eq. (42) is replaced by  $v_{F,ab}$ . The weight functions for the half-torus and the spherical Fermi surface are shown in Fig. 3. For the half-torus  $\nu = 4$  (appropriate for MgB<sub>2</sub>) has been chosen.  $g_F(s)$  for the half-torus starts with a finite value at  $s = 0$ . This has a topological reason: on the half-torus with field in  $c$ -axis direction there exist two lines of points at which the Fermi velocity is parallel to the magnetic field. At these points the projection of the Fermi velocity onto the plane perpendicular to the field vanishes. In contrast, for the spherical and elliptical Fermi surfaces there exist only two such points, the poles. Therefore  $g_F(s)$  becomes 0 at  $s = 0$  and increases linearly. For the cylindrical Fermi surface no such points exist and  $g_F(s)$  becomes 0 for  $s \neq 1$ .

In Fig. 4 we show the density of states for the half-torus for different field strengths in  $c$ -axis direction. Because of the finite value of  $g_F(s)$  for  $s = 0$  in this case there is large weight to the BCS singularity of the spectrum at  $B = 0$ .

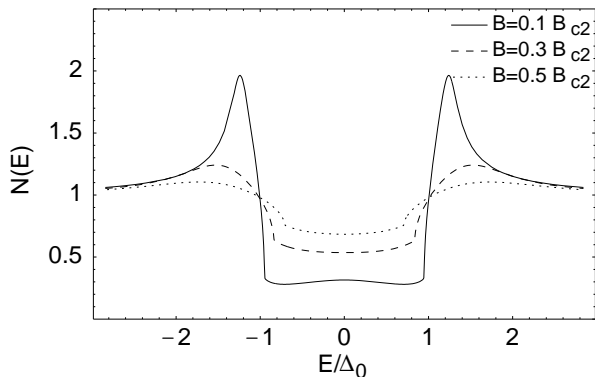


FIG. 5: Averaged density of states for spherical and elliptical Fermi surface, respectively, with magnetic field parallel to the  $c$ -axis direction

This results in the sharp flank at the gap edge seen in Fig. 4 even for higher magnetic fields. The position of the sharp flank closely follows the field dependence of the gap. The singularity itself is washed out by the averaging process. But still the most important contribution comes from the highest field, corresponding to  $s = 1$  in Fig. 3.

The characteristic function of the spherical Fermi surface increases linearly from  $s = 0$ . This results in a visible break at the gap edge in the density of states but no longer in a significant flank, as shown in Fig. 5. Again, the most important contribution comes from the highest fields ( $s = 1$ ), leading to a peak-to-peak distance that increases with increasing magnetic field. The reduction of the BCS singularity is less pronounced than for the half-torus, because the weight near  $s = 1$  in  $g_F(s)$  (Fig. 3) is stronger for the sphere than for the half-torus.

### B. Field in $ab$ -plane direction

In order to calculate the characteristic function  $g_F(s)$  for field directed in  $ab$ -plane direction it is necessary to take into account the vortex lattice distortion via the parameter  $\tau$ . For each value of the magnetic field  $\tau$  has to be found by minimizing the free energy of the system as described in section II. This makes the calculation of  $g_F(s)$  more involved in this case. However, even without knowing the value of  $\tau$  one can get already insight into the shape of the characteristic function  $g_F(s)$  by analyzing the extrema and saddle points of  $|\eta_{k_F}|$  in Eqs. (36) and (37). Via Eq. (41) these saddle points will lead to van Hove singularities in  $g_F(s)$ .

For the cylindrical Fermi surface we find from Eq. (36) that there is a minimum at  $|\eta_{k_F}|(\varphi = \pi/2, k_c = 0) = 0$ , a maximum at  $|\eta_{k_F}|(\varphi = 0, ck_c = \pi/2)/\alpha = \sqrt{e^{2\tau} + e^{-2\tau}\epsilon_c^2}$ , and two saddle points at  $|\eta_{k_F}|(\varphi = 0, k_c = 0)/\alpha = e^\tau$  and  $|\eta_{k_F}|(\varphi = \pi/2, ck_c = \pi/2)/\alpha = e^{-\tau}\epsilon_c$  leading to logarithmic singularities. In this case we can show analytically that  $\tau$  is minimized by  $e^\tau = \sqrt{\epsilon_c}$

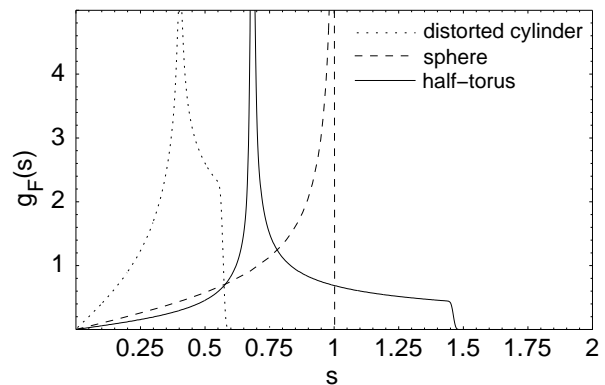


FIG. 6: The characteristic functions  $g_F(s)$  for the cylindrical, spherical and half-toroidal Fermi surface. The magnetic field is applied in  $ab$ -plane direction.

for all field strengths. Therefore, the two saddle points collapse into one. The characteristic functions obtained after minimization of  $\tau$  are shown in Fig. 6 for field in  $ab$ -plane direction. The dotted line shows the result for the distorted cylinder. The logarithmic van Hove singularity due to the two saddle points is seen at  $s = \sqrt{\epsilon_c} \simeq 0.4$  and a step due to the maximum is found at  $s = \sqrt{2}\epsilon_c \simeq 0.57$ .

For the other three Fermi surfaces from Eq. (37) we find a minimum at  $|\eta_{k_F}|(\varphi = \pi/2, \vartheta = 0) = 0$  and two extremal points at  $|\eta_{k_F}|(\vartheta = \pi/2)/\alpha = e^{-\tau}$  and  $|\eta_{k_F}|(\varphi = 0, \vartheta = 0)/\alpha = e^\tau$ . The point at  $|\eta_{k_F}|/\alpha = e^{-\tau}$  for  $\tau > 0$  turns out to be an extended saddle point, leading to a square-root singularity in  $g_F(s)$ . In the case of a spherical or elliptical Fermi surface  $\tau = 0$  or  $\bar{\tau} = 0$  is found due to symmetry, respectively. As we have noted before, both the gap amplitude and the free energy functional depend on  $\tau$  only via  $|\eta_{k_F}|$ . Also, as we have shown in Eq. (40), we can bring  $|\eta_{k_F}|$  of the elliptic Fermi surface into the same form as  $|\eta_{k_F}|$  of the spherical Fermi surface with  $\tau$  substituted by  $\bar{\tau}$  and  $v_F$  substituted by  $\sqrt{v_{F,ab}v_{F,c}}$ . In this case the two extremal points again collapse into one and we just rediscover the same function  $g_F(s)$  as for field in  $c$ -axis direction, as expected. For the half-torus the parameter  $\tau$  is nonzero and field dependent, however. Therefore, a square-root singularity is seen in Fig. 6 at  $s = e^{-\tau}$  and a step due to the maximum at  $s = e^\tau$ . Here,  $g_F(s)$  is shown for high fields close to  $B_{c2}$  where we find  $\tau = 0.375$ .

In Figs. 7 and 8 we show the corresponding densities of states for cylindrical and toroidal Fermi surface, respectively. For this field direction the densities of states for spherical (Fig. 5), distorted cylindrical (Fig. 7), and toroidal (Fig. 8) Fermi surfaces appear to be much more similar to each other. This becomes clear from the similarity of the characteristic functions in Fig. 6: all curves increase linearly at low values of  $s$ . Again, the reason for this is topological: for field applied in  $ab$ -plane direction in all three cases there exist a few singular points on

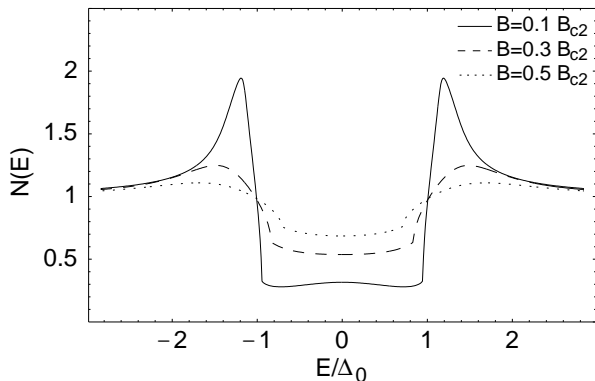


FIG. 7: Averaged density of states for the distorted cylinder with magnetic field in  $ab$ -plane direction

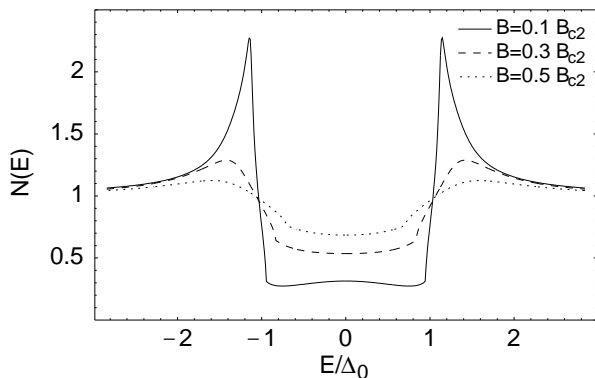


FIG. 8: Averaged density of states for the half-torus with magnetic field applied in  $ab$ -plane direction

the Fermi surfaces at which the Fermi velocity is directed parallel to the magnetic field, in contrast to the case of field applied in  $c$ -axis direction. Accordingly, the results in Figs. 7 and 8 resemble that of the spherical Fermi surface and we can identify again the characteristic break at the gap edge and the distinct peaks on each side of the gap that we have already recognized in Fig. 5.

## V. COMPARISON WITH A BROADENED BCS TYPE DENSITY OF STATES

In analysis of experimental tunneling data on superconductors in the vortex state a simple model of a BCS type density of states with a broadening parameter  $\Gamma$  of the following form has been used frequently<sup>4,5,7,17,18</sup>

$$N(E) = \text{Re} \left[ \frac{E + i\Gamma}{\sqrt{(E + i\Gamma)^2 - \Delta^2}} \right] \quad (52)$$

for  $E > 0$ . Here,  $\Delta$  and  $\Gamma$  have been used as field dependent fitting parameters. In this section we want to make

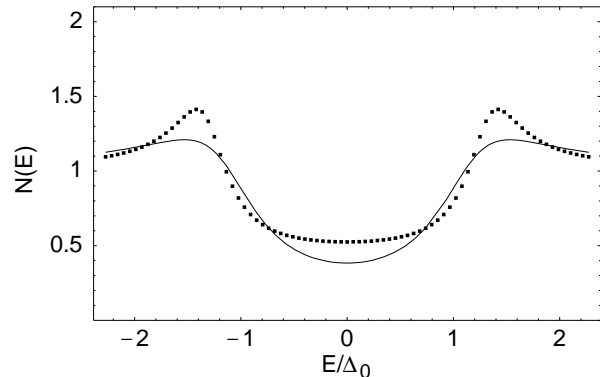


FIG. 9: Spatially and momentum averaged density of states for  $B = 0.3 B_{c2}$ . The boxes show the data from the quasi-classical calculation (also seen in Fig. 2) and the solid line represents the broadened BCS spectrum that was fitted to these data using Eq. (52).

a critical comparison of this model with our results and point out the limitations of this model.

Looking at Figs. 2, 4, and 5 it is immediately apparent that Eq. (52) is certainly not able to reproduce these very different shapes of the curves, because the results in Figs. 2, 4, and 5 are shown for the same reduced magnetic field and gap values (only the Fermi surface structure was changed). Nevertheless one might ask whether these curves can be approximated by Eq. (52) with some effective broadening parameter  $\Gamma$ . In order to answer this question we have made least squares fits of Eq. (52) to our results for the cylindrical Fermi surface Eq. (47) shown in Fig. 2. In Fig. 9 we show the best fit for  $B = 0.3 B_{c2}$ . It appears that the width of the peaks at the gap edge and the high value of the density of states at small energies cannot be described simultaneously very well. The main reason for this failure is due to the presence of a high amount of vortex core states that dominate at low energies and cannot be captured very well by Eq. (52).

In Fig. 10 we show the values of the two parameters  $\Delta$  and  $\Gamma$  as a function of magnetic field found from our fits (solid squares). In the upper panel we compare  $\Delta(B)$  with the actual field dependence of the gap shown as the solid line. This comparison shows that the gap value extracted from Eq. (52) does not very accurately reproduce the actual gap value and care should be taken when interpreting gap values extracted this way. The lower panel in Fig. 10 shows the field dependence of the broadening parameter  $\Gamma$ . It is clear that this quantity increases with increasing magnetic field. For illustration we are also showing the 'average Doppler shift'  $|\eta_{k_F}|/\sqrt{2}$  as the solid line. This quantity represents the average energy broadening due to the local Doppler shift of the energies of the excited quasiparticles in the presence of the supercurrents around the vortices. The comparison shows that  $\Gamma$  roughly measures this average Doppler shift, particularly at higher magnetic fields.



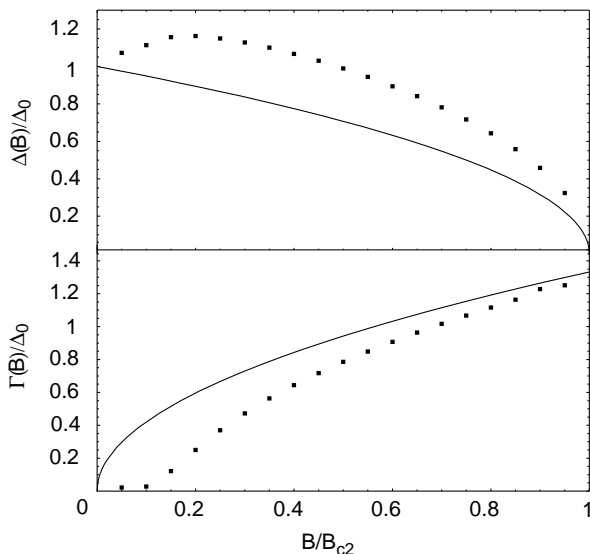


FIG. 10: The upper panel shows the gap amplitude that was extracted from the fitting process (boxes) in comparison with the field dependence of the gap function that was used to calculate the quasiclassical spectra (solid line). The lower panel shows the variation of the fitting parameter  $\Gamma$  (boxes) as a function of the magnitude of the magnetic field compared with the average Doppler shift  $|\eta_{k_F}|/\sqrt{2}$  (solid lines).

Instead of using Eq. (52) for an extraction of the magnetic field dependence of the gap from experimental data it would be better to use the theory presented here. This requires a priori knowledge of the Fermi surface structure, however. For the special but important case of the cylindrical Fermi surface with field in  $c$ -axis direction the calculation simplifies and we can suggest an improved version of Eq. (52): first we note that Eq. (47) depends on magnetic field only through the field dependence of the gap function  $\Delta(B)$  and the quantity  $\alpha \propto \sqrt{B}$ . Therefore, Eq. (47) can be brought into the following convenient form:

$$N(B, E) = \text{Re} \left[ \frac{1}{\sqrt{1 + P_\Lambda(B, E)}} \right] \quad (53)$$

with

$$P_\Lambda(B, E) = 2 \frac{\bar{B}}{B} \left( \frac{\Delta(B)}{\Delta_0} \right)^2 (1 + i\sqrt{\pi} x w(x + i0^+)) \quad (54)$$

and

$$x = iz = \sqrt{\frac{\bar{B}}{B}} \frac{E}{\Delta_0} \quad (55)$$

where we have introduced a characteristic magnetic field

$$\bar{B} = \frac{2c}{\hbar v_F^2 e} \Delta_0^2 \quad (56)$$

such that  $\sqrt{\frac{\bar{B}}{B}} = \frac{\alpha}{\sqrt{2}\Delta_0}$ . In Eq. (53) all material dependent quantities including the Fermi surface structure appear lumped into the single parameter  $\bar{B}$ , which makes Eq. (53) particularly useful for fitting of experimental data. Such a fitting could proceed as follows: first, the zero field value  $\Delta_0$  has to be extracted from a usual fit to zero field experimental data. Then, Eq. (53) can be fitted to finite field data using  $\bar{B}$  as a field independent and  $\Delta(B)/\Delta_0$  as a field dependent fitting parameter. For this fitting procedure a useful approximation of the expression in Eq. (54) containing Dawson's integral for real values of  $x$  is given by

$$1 + i\sqrt{\pi} x w(x + i0^+) \simeq \frac{1 - x^2 - 0.2x^4}{1 + x^2 + 0.4x^6} + i\sqrt{\pi} x e^{-x^2} \quad (57)$$

This approximation is better than 2% and reproduces the behavior of the left hand side in the limit  $x \rightarrow 0$  to order  $x^2$  and in the limit  $x \rightarrow \infty$  to order  $1/x^2$ .

In order to get some feeling for the parameter  $\bar{B}$ , we can relate it to the upper critical field  $B_{c2}$  using the linearized gap equation. At  $B_{c2}$  we find<sup>12</sup>

$$\alpha(B_{c2}) = \sqrt{2\gamma}\Delta_0 \exp \left\{ - \left\langle \ln \frac{|\eta_{k_F}|}{\alpha} \right\rangle_{FS} \right\} \quad (58)$$

and therefore

$$\frac{\bar{B}}{B_{c2}} = \left( \frac{\sqrt{2}\Delta_0}{\alpha(B_{c2})} \right)^2 = \frac{\exp \left\{ 2 \left\langle \ln \frac{|\eta_{k_F}|}{\alpha} \right\rangle_{FS} \right\}}{\gamma} \quad (59)$$

For the cylindrical Fermi surface with field in  $c$ -axis direction considered here  $\frac{|\eta_{k_F}|}{\alpha} = 1$  and therefore we have  $\bar{B} = B_{c2}/\gamma = 0.561B_{c2}$ .

## VI. APPLICATION TO $\text{MgB}_2$

In this section we want to apply our findings to the situation in  $\text{MgB}_2$ . It has been established recently that this compound belongs to the rare case of a superconductor possessing two different sized gaps on two different parts of the Fermi surface: a large gap living on the cylindrical  $\sigma$ -bands and a small gap on the three-dimensional  $\pi$ -bands.<sup>19,20,21,22</sup> The structure of the  $\pi$ -band Fermi surface can be approximated by a half-torus as pointed out in Ref. 12. The quasiparticle excitations in the vortex state of  $\text{MgB}_2$  have been studied recently by tunneling spectroscopy<sup>4,5,6,22</sup> and the field dependence of the superconducting gap was extracted.<sup>4,5,6</sup>

The normalized total density of states of a two band superconductor is given by a weighted average of the two partial densities of states for each of the two bands:

$$N(B, E) = (1 - w_\pi)N_\sigma(B, E) + w_\pi N_\pi(B, E) \quad (60)$$

Here,  $w_\pi$  is the weight of the  $\pi$ -band density of states and has been calculated by band structure calculations<sup>19,23</sup> to

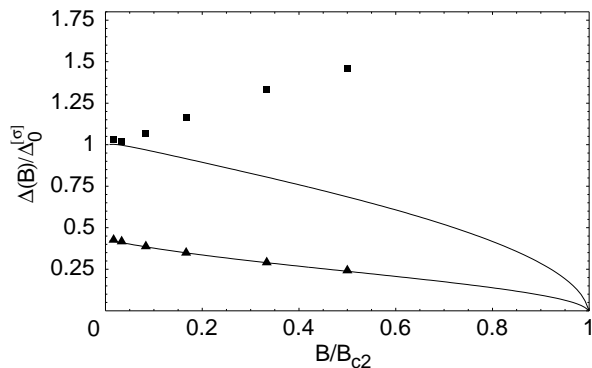


FIG. 11: The two gaps of MgB<sub>2</sub> as a function of magnetic field. The solid squares show the maxima of the peaks that result from the  $\sigma$  band density of states, the triangles mark the flanks of the smaller gaps, also extracted from the quasi-particle spectrum.

be  $w_\pi = 0.577$ . For the partial densities of states we can take our results from section IV for the distorted cylinder with the distortion parameter  $\epsilon_c = 0.163$  and the half-torus  $\nu = 4$ . The two different gap amplitudes have to be found from a solution of the two by two gap equation in the vortex state:

$$\Delta^\alpha(\vec{r}) = \pi T \sum_{\alpha'} \sum_{|\epsilon_n| < \omega_c} \lambda^{\alpha, \alpha'} \left\langle f^{\alpha'}(\vec{r}, \vec{k}_{F_\alpha}, i\epsilon_n) \right\rangle_{FS} \quad (61)$$

where we assumed an isotropic pairing interaction  $\lambda^{\alpha, \alpha'}$  with  $\alpha$  the band index:  $\alpha = \sigma, \pi$ .

In Fig. 11 the two gap amplitudes are shown as function of the applied magnetic field for the set of parameters used in Ref. 12. The resulting density of states for field in  $c$ -axis direction is shown in Fig. 12. From this figure it becomes apparent that the peak at the gap edge of the small gap is much more rapidly suppressed as the field is increased. This is due to the topology of the  $\pi$ -band: as we have shown in the previous section its half-torus shape leads to a much more rapid suppression of the peak at the gap edge than for the cylindrical Fermi surface of the  $\sigma$ -band. Experimentally, this effect has been noted by Gonnelli et al.<sup>4</sup> Already at comparatively low fields of about 1 Tesla no apparent structure of the  $\pi$ -band gap could be observed anymore, while the structure of the  $\sigma$ -band gap remains visible to much higher fields of about 4-5 Tesla.

For comparison in Fig. 11 we are showing the position of the peak in the  $\sigma$ -band density of states as a function of magnetic field as the solid squares. The position of the sharp flanks in the  $\pi$ -band density of states is shown as the triangles. Clearly, the structures in the densities of states are behaving quite differently in the two bands due to their different topologies. This effect should be taken into account when analyzing the experimental data.

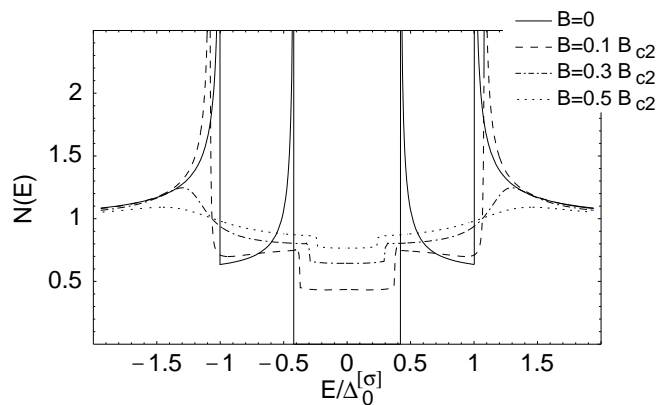


FIG. 12: Averaged density of states for MgB<sub>2</sub> with magnetic field parallel to the  $c$ -axis direction of the crystal lattice, calculated as a weighted sum of the averaged density of states of a toroidal Fermi surface and a cylindrical Fermi surface using Eq. (60). Results are shown for different magnetic fields.

## VII. CONCLUSIONS

We studied the influence of Fermi surface topology on the density of states in the vortex state of type II superconductors for the four Fermi surface structures shown in Fig. 1. The topology of the Fermi surface takes influence on the density of states, because the direction of the Fermi velocity with respect to the local supercurrent flow around the vortices leads to a change of the excitation energy of the quasiparticles. We saw that the density of states behaves quite differently for cylindrical, spherical and toroidal Fermi surfaces. The field dependence and shape of the curves shows characteristic features related to the topology of the Fermi surface in question. We showed that these features can be understood in terms of characteristic Fermi surface functions. A particularly important role is played by the number of points on the Fermi surface at which the Fermi velocity is directed parallel to the external magnetic field.

We compared our results with the simple model of a broadened BCS type density of states, that has been used frequently in the past for analysis of experimental data. This comparison showed that the contribution coming from vortex core states is underestimated in this simple model. This leads to inaccuracies in the gap values extracted from the broadened BCS model. For the special case of a cylindrical Fermi surface with field along the  $c$ -axis direction, we suggested an improved formula for the density of states in the vortex state, in which all material properties are lumped into a single parameter. This new formula does not possess the limitations of the broadened BCS model and can be used for fits to experimental data.

We applied our results to the case of the two gap superconductor MgB<sub>2</sub>. This case is particularly interesting,

because the two Fermi surfaces related to the two gaps possess completely different topology. We demonstrated that this leads to very different field dependencies of the partial densities of states, resembling recent observations on this compound.

### Acknowledgments

We would like to thank M. Eskildsen and R. Gonnelli for valuable discussions. S. Graser acknowledges support through the 'Graduiertenförderungsprogramm des Landes Baden-Württemberg'.

## APPENDIX A: CALCULATION OF THE FREE ENERGY

In this Appendix we provide a derivation of Eq. (15) for the free energy difference within the method we are using here. The difference of the free energy between the superconducting state and the normal state for the case of an even parity superconductor can be calculated by the coupling constant integration method<sup>25</sup>

$$\Omega_S - \Omega_N = \int_0^1 \frac{d\lambda}{\lambda} \langle \lambda H_{int} \rangle_\lambda \quad (\text{A1})$$

where  $H_{int}$  denotes the interaction Hamiltonian. For a multiband superconductor this equation can be expressed in terms of the gap function  $\tilde{\Delta}^\alpha(\vec{r}, \vec{k}_F; \lambda)$  and the anomalous Eilenberger propagator  $\tilde{f}^\alpha(\vec{r}, \vec{k}_F, i\epsilon_n; \lambda)$  corresponding to a reduced pairing interaction  $\lambda \cdot V^{\alpha\alpha'}(\vec{k}_F, \vec{k}'_F)$

$$\Omega_S - \Omega_N = - \int_0^1 \frac{d\lambda}{\lambda} \int_{C_\Lambda} \frac{d^2r}{|C_\Lambda|} \sum_\alpha \left\langle \left[ \tilde{\Delta}^\alpha(\vec{r}, \vec{k}_F; \lambda) \right]^\dagger \times \pi T \sum_{|\epsilon_n| < \omega_c} \tilde{f}^\alpha(\vec{r}, \vec{k}_F, i\epsilon_n; \lambda) \right\rangle_{FS_\alpha} \quad (\text{A2})$$

Here,  $\alpha$  is the band index and  $\tilde{\Delta}^\alpha(\vec{r}, \vec{k}_F; \lambda)$  is solution of the renormalized gap equation

$$\tilde{\Delta}^\alpha(\vec{r}, \vec{k}_F; \lambda) = \lambda \sum_{\alpha'} \left\langle V^{\alpha\alpha'}(\vec{k}_F, \vec{k}'_F) \pi T \sum_{|\epsilon_n| < \omega_c} \tilde{f}^{\alpha'}(\vec{r}, \vec{k}'_F, i\epsilon_n; \lambda) \right\rangle_{FS'_{\alpha'}} \quad (\text{A3})$$

Here,  $\tilde{f}^{\alpha'}(\vec{r}, \vec{k}'_F, i\epsilon_n; \lambda)$  is a solution of the Eilenberger equation Eq. (1) in the presence of the  $\lambda$ -dependent gap function  $\tilde{\Delta}^\alpha(\vec{r}, \vec{k}_F; \lambda)$  and depends on the parameter  $\lambda$  only implicitly via  $\tilde{\Delta}^\alpha$ . The integration over  $\lambda$  in Eq. (A2) can be substituted by an integration over the pairing potential, a usual technique as described in textbooks.<sup>25</sup> Generalizing this to the case of an inhomogeneous superconductor we introduce a function  $x(\lambda)$  via

$$x(\lambda) \cdot \Delta^\alpha(\vec{r}, \vec{k}_F) = \tilde{\Delta}^\alpha(\vec{r}, \vec{k}_F; \lambda) \quad (\text{A4})$$

Then,  $\tilde{f}^\alpha$  can be viewed as a function of  $x$ , calculated for a reduced gap  $x\Delta^\alpha$ , and the integration over  $\lambda$  can be substituted by an integration over  $x$ . In order to do so, we insert Eq. (A4) into Eqs. (A2) and (A3). Taking the derivative of Eq. (A3) with respect to  $x$  we find

$$\frac{x}{\lambda} \frac{d\lambda}{dx} \Delta^\alpha(\vec{r}, \vec{k}_F) = \Delta^\alpha(\vec{r}, \vec{k}_F) - \lambda \sum_{\alpha'} \left\langle V^{\alpha\alpha'}(\vec{k}_F, \vec{k}'_F) \pi T \sum_{|\epsilon_n| < \omega_c} \frac{d\tilde{f}^{\alpha'}}{dx}(\vec{r}, \vec{k}'_F, i\epsilon_n; x) \right\rangle_{FS'_{\alpha'}} \quad (\text{A5})$$

Inserting the hermitian conjugate of Eq. (A5) into Eq. (A2) and using the fact that the pairing interaction is hermitian, i.e.

$$\left[ V^{\alpha\alpha'}(\vec{k}_F, \vec{k}'_F) \right]^\dagger = V^{\alpha'\alpha}(\vec{k}'_F, \vec{k}_F) \quad (\text{A6})$$

we arrive at

$$\Omega_S - \Omega_N = - \int_{C_\Lambda} \frac{d^2r}{|C_\Lambda|} \sum_\alpha \left\langle \pi T \sum_{|\epsilon_n| < \omega_c} \int_0^1 dx \left\{ \left[ \Delta^\alpha(\vec{r}, \vec{k}_F) \right]^\dagger \tilde{f}^\alpha(\vec{r}, \vec{k}_F, i\epsilon_n; x) - \Delta^\alpha(\vec{r}, \vec{k}_F) \left[ x \frac{d\tilde{f}^\alpha}{dx}(\vec{r}, \vec{k}_F, i\epsilon_n; x) \right]^\dagger \right\} \right\rangle_{FS_\alpha} \quad (\text{A7})$$

A partial integration of the last term with respect to  $x$  finally yields

$$\Omega_S - \Omega_N = \int_{C_\Lambda} \frac{d^2r}{|C_\Lambda|} \sum_\alpha \left\langle \pi T \sum_{|\epsilon_n| < \omega_c} \text{Re} \left\{ \left[ \Delta^\alpha(\vec{r}, \vec{k}_F) \right]^\dagger \left( f^\alpha(\vec{r}, \vec{k}_F, i\epsilon_n) - 2 \int_0^1 dx \tilde{f}^\alpha(\vec{r}, \vec{k}_F, i\epsilon_n; x) \right) \right\} \right\rangle_{FS_\alpha} \quad (\text{A8})$$

This equation still holds generally for inhomogeneous multiband superconductors.

We can now employ the approximation procedure introduced in Ref. 14 and evaluate the spatial average in Eq. (A8). For a single band superconductor we find

$$\frac{1}{|C_\Lambda|} \int_{C_\Lambda} d^2r \left[ \Delta(\vec{r}, \vec{k}_F) \right]^\dagger \tilde{f}(\vec{r}, \vec{k}_F, i\epsilon_n; x) = \frac{|\Delta(\vec{k}_F)|^2}{\epsilon_n} \sqrt{\pi} z w(iz) \frac{x}{\sqrt{1 + x^2 P_\Lambda(\vec{k}_F, i\epsilon_n)}} \quad (\text{A9})$$

The first term in Eq. (A8) is obtained for  $x = 1$ , of course. In this expression  $z$  denotes the normalized Matsubara frequencies as introduced in Eq. (9). Using the same method Eq. (16) can be derived from Eq. (A3) for  $\lambda = 1$  averaging over a unit cell of the vortex lattice and eliminating the pairing interaction  $V$  using the linearized gap equation at  $T = T_c$ . Finally, the integration over  $x$  in Eq. (A8) can be carried out analytically using Eq. (A9) and we obtain the result in Eq. (15).

- 
- <sup>1</sup> K. Izawa, H. Takahashi, H. Yamaguchi, Y. Matsuda, M. Suzuki, T. Sasaki, T. Fukase, Y. Yoshida, R. Settai, and Y. Onuki, *Phys. Rev. Lett.* **86**, 2653 (2001).
- <sup>2</sup> B. W. Hogenboom, K. Kadowaki, B. Revaz, M. Li, C. Renner, and Ø. Fischer, *Phys. Rev. Lett.* **87**, 267001 (2001).
- <sup>3</sup> K. Maki, P. Thalmeier, and H. Won, *Phys. Rev. B* **65**, 140502 (2002).
- <sup>4</sup> R. Gonnelli et al, cond-mat/0308152 and cond-mat/0305560.
- <sup>5</sup> Y. Bugoslavsky et al, cond-mat/0307540.
- <sup>6</sup> T. Ekino, T. Takasaki, T. Muranaka, J. Akimitsu, and H. Fujii, *Phys. Rev. B* **67**, 094504 (2003).
- <sup>7</sup> Y. G. Naidyuk, R. Häussler, and H. v. Löhneysen, *Physica B* **218**, 122 (1996).
- <sup>8</sup> G. E. Volovik, *JETP Lett.* **58**, 469 (1993).
- <sup>9</sup> K. A. Moler, D. J. Baar, J. S. Urbach, R. Liang, W. N. Hardy, and A. Kapitulnik, *Phys. Rev. Lett.* **73**, 2744 (1994).
- <sup>10</sup> B. Revaz, J.-Y. Genoud, A. Junod, K. Neumaier, A. Erb, and E. Walker, *Phys. Rev. Lett.* **80**, 3364 (1998).
- <sup>11</sup> K. Maki in *Superconductivity*, ed. R. D. Parks, Marcel Dekker (New York 1969).
- <sup>12</sup> T. Dahm and N. Schopohl, *Phys. Rev. Lett.* **91**, 017001 (2003).
- <sup>13</sup> W. Pesch, *Z. Phys. B* **21**, 263 (1975); P. Klimesch and W. Pesch, *J. Low Temp. Phys.* **32**, 869 (1978).
- <sup>14</sup> T. Dahm, S. Graser, C. Iniotakis, and N. Schopohl, *Phys. Rev. B* **66**, 144515 (2002).
- <sup>15</sup> G. Eilenberger, *Z. Phys.* **214**, 195 (1968).
- <sup>16</sup> A. I. Larkin and Yu. N. Ovchinnikov, *Zh. Eksp. Teor. Fiz.* **55**, 2262 (1968) - engl. transl. *Sov. Phys. JETP* **28**, 1200 (1969).
- <sup>17</sup> Y. G. Naidyuk, H. v. Löhneysen, and I. K. Yanson, *Phys. Rev. B* **54**, 16077 (1996).
- <sup>18</sup> R. C. Dynes, J. P. Garno, G. B. Hertel, and T. P. Orlando, *Phys. Rev. Lett.* **53**, 2437 (1984).
- <sup>19</sup> A. Y. Liu, I. I. Mazin, and J. Kortus, *Phys. Rev. Lett.* **87**, 087005 (2001).
- <sup>20</sup> H. J. Choi, D. Roundy, H. Sun, M. L. Cohen, and S. G. Louie, *Nature(London)* **418**, 758 (2002).
- <sup>21</sup> B. B. Jin, T. Dahm, A. I. Gubin, E.-M. Choi, H. J. Kim, S.-I. Lee, W. N. Kang and N. Klein, cond-mat/0304051 to appear in *Phys. Rev. Lett.*
- <sup>22</sup> M. R. Eskildsen, M. Kugler, S. Tanaka, J. Jun, S. M. Kazakov, J. Karpinski, and Ø. Fischer, *Phys. Rev. Lett.* **89**, 187003 (2002).
- <sup>23</sup> J. Kortus, I. I. Mazin, K. D. Belashchenko, V. P. Antropov, and L. L. Boyer, *Phys. Rev. Lett.* **86**, 4656 (2001).
- <sup>24</sup> T. Dahm, S. Graser, and N. Schopohl, cond-mat/0304194.
- <sup>25</sup> A. A. Abrikosov, L. P. Gorkov, and I. E. Dzyaloshinski, *Methods of Quantum Field Theory in Statistical Physics*, Dover (New York 1975).